Chapter 5

Adsorption and dissociation of O_2 on Pt(553)

Abstract

Molecular adsorption and dissociation of O_2 on Pt(553) have been investigated using supersonic molecular beam techniques and TPD. The sticking probability was determined for various combinations of incident kinetic energy, surface temperature, incident angle, and surface coverage. A comparison with data for Pt(533) and Pt{110}(1x2) shows quantitatively the same high step-induced sticking at low energies compared to Pt(111). The enhancement is therefore insensitive to the exact arrangement of atoms forming surface corrugation. We consider energy transfer and electronic effects to explain the enhanced sticking. On the other hand, dissociation dynamics at higher incident energies are strongly dependent on step type. The Pt(553) and Pt(533) surfaces are more reactive than Pt(111), but the (100) step shows higher sticking than the (110) step. We relate this difference to a variation in the effective lowering of the barrier to dissociation from molecularly adsorbed states into atomic states. Our findings are in line with results from experimental desorption studies and theoretical studies of atomic binding energies. We discuss the influence of the step type on sticking and dissociation dynamics with a 1-D PES.

This chapter is based on: L. Jacobse, A. den Dunnen, and L.B.F. Juurlink, *J. Chem. Phys.*, 2015, **143**, 014703.

5.1 Introduction

Platinum is widely used as a catalyst for a variety of chemical processes, including oxidation reactions and the conversion of car exhaust gases. One of the most important steps in oxidation reactions is breaking the oxygen-oxygen bond in O_2 by dissociative adsorption. Therefore, a thorough understanding of the O_2/Pt system is of crucial importance to describe the overall process of oxidation. By combining single crystal surfaces in an ultra-high vacuum (UHV) environment with supersonic molecular beam techniques, detailed information about the role of surface structure and other variables, e.g. incident kinetic energy (E_i), surface temperature (T_s), incident angle (Φ), and coverage (θ) can be obtained. Especially the flat Pt(111) surface has drawn a lot of attention in the past years[19–21,23,24,75–81]. However, other low-Miller-index surfaces, e.g. Pt{100}(1x1)[82] and Pt{110}(1x1)[83], corrugated surfaces, e.g. Pt(533)[84–86] and other stepped surfaces[87–92], and reconstructed surfaces, e.g. Pt{110}(1x2)[69] and Pt(100)hex-R0.7°[93], have also been studied both experimentally and theoretically.

As reviewed by Vattuone *et al.*, four different adsorption states of oxygen on Pt(111) have been identified experimentally[94]. A molecular physisorbed state, two molecular chemisorbed states (peroxo- and superoxo-like), and one atomically chemisorbed state have been observed using various spectroscopic techniques. Theoretical studies show three different molecular adsorption states for O_2 on Pt(111). A top-bridge-top (superoxo-like), a top-fcc-bridge (peroxo-like), and a top-hcp-bridge orientation are suggested[77]. Adsorption on a top-hcp-bridge site was not observed experimentally. This is explained by the low barrier for rotation to the superoxo species. Dissociation of the molecularly chemisorbed species was only observed with the peroxo or top-hcp-bridge species as intermediate state. Depending on the surface coverage, the most stable adsorption sites for the O atoms were the fcc and hcp sites (low coverage) or just the fcc sites (all coverages). A series of molecular beam studies have investigated the dissociation dynamics of O_2 on Pt(111)[19,21,24,92].

Surfaces containing (111) terraces with regular steps are often used to model the influence of edges occurring on real catalytic particles. Figure 5.1 shows several of such surfaces in comparison to the (111) plane. Step 'defects' are expected to play an active role in O_2 dissociation dynamics on platinum. Gee and Hayden investigated O_2 adsorption on the Pt(533) surface[84]. This surface consists of four-

atom wide (111) terraces separated by square (100) step edges (Pt[4(111)x(100)]). Walker *et al.* studied the reconstructed Pt{110}(1x2) surface (figure 5.1d), which contains of three-atom wide (111) terraces separated by sharp (111) type step edges[69].

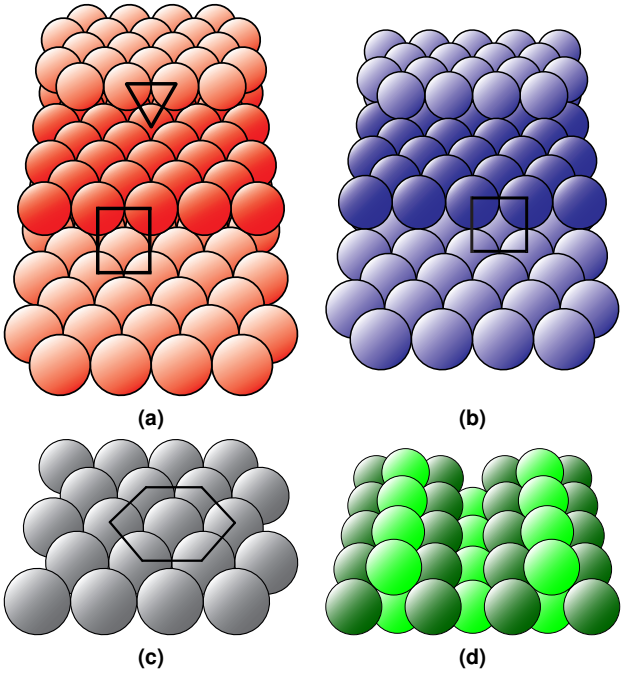

Figure 5.1: a) The Pt(553) surface structure with hexagonal terraces and rectangular (or triangular) step sites; b) The Pt(533) surface structure with hexagonal terraces and square step sites; c) The Pt(111) surface with a hexagonal structure; d) The Pt{110}(1x2) surface structure with a missing row reconstruction.

For surfaces consisting of (111) terraces, we have demonstrated that the step type is a relevant parameter in the desorption process[95]. This temperature programmed desorption (TPD) study of the O_2 associative desorption from Pt(553) (figure 5.1a) and Pt(533) (figure 5.1b) showed significantly different desorption temperatures for the steps while desorption from the (111) terraces occurred at the same temperature. Desorption of the molecularly chemisorbed species occurs around the same temperature for the different step types as was shown by experiments for Pt(331)[90] and Pt(311)[91]. Density functional theory (DFT) calculations find similar characteristics[87].

To study the influence of step type on adsorption experimentally, one may compare results for the previously mentioned molecular beam studies for Pt(533) and Pt{110}(1x2). However, as these surfaces have different terrace lengths and different step types, a better comparison is made with Pt(553) (Pt[4(111)x(110)]). This surface has the same terrace width as Pt(533), only now with rectangular (110) step edges. Alternatively, Pt(553) can be described as a surface with five-atom wide (111) terraces and (111) type step edges (Pt[5(111)x(111)]). Both the rectangular and triangular atomic arrangements at the step are indicated in figure 5.1a. In this regard, Pt(553) may also be compared better to Pt{110}(1x2) as both contain the same arrangement of Pt atoms forming the step edge.

Here, we report on studies of the molecular dynamics of adsorption and dissociation of O_2 on Pt(553). The overlap in surface structure allows for a fair comparison of our data to those published for Pt(111)[20] and Pt(533)[84]. As far as data are available, a comparison is also made to the data for Pt{110}(1x2)[69].

5.2 Experimental

Experiments were performed using an UHV apparatus (base pressure $< 1 \cdot 10^{-10}$ mbar) equipped with, among others, a double differentially pumped supersonic molecular beam, a fixed quadrupole mass spectrometer (Pfeiffer, QMA 200), a quadrupole mass spectrometer (UTI, 100C) which can be moved along the molecular beam axis, and a LEED/Auger (RVL 2000/8/R) apparatus. The Pt(553) single crystal (cut and polished $< 0.1^\circ$, Surface Preparation Laboratory, Zaandam, The Netherlands) is suspended from a liquid nitrogen cooled cryostat on an x, y, z, θ manipulator. It was cleaned by repeated cycles of Ar^+ bombardment (Messer, 5.0; 15 μA, 5 min.), annealing at a surface temperature of 900 K in an oxygen atmosphere (Messer, 5.0; $3.5 \cdot 10^{-8}$ mbar, 3 min.), and three minutes of vacuum annealing at a surface temperature of 1200 K. The surface cleanliness was confirmed by comparison of TPD spectra with ones that have been measured previously in our group and are known to be sensitive to structure and contamination[95]. Surface structure was confirmed by LEED. The spot row spacing to spot splitting ratio was found to be $\sim$3.9, which corresponds well to the literature value of 3.8406[96]. In between measurements, the crystal was vacuum annealed for 3 min. at a surface temperature of 1200 K. Consistency of the quality of the Pt(553) surface during the

day was monitored by regularly repeating an experiment under identical conditions. For angle-dependence studies, the rotational axis of our crystal would ideally be along the $[\bar{1}10]$ direction. We determined it to be off by 15°. Upon rotation of the crystal, molecules do not impinge exactly orthogonally into the step edge.

The molecular beam was created by expansion of a gas at 0.5-4.3 bar through a tungsten nozzle with a circular 45 μm diameter orifice. A beam is shaped by a set of skimmers. Flags and a chopper wheel allow us to modulate the beam. The kinetic energy of the molecular beam was controlled by seeding or antiseeding with helium (Linde, 6.0) or argon (Air Products, 5.7). The nozzle is concentrically placed in a larger diameter tube. The tube is heated by electron bombardment from two filaments, radiatively heating the nozzle and leading to higher kinetic energies of the molecular beam. By combining antiseeding and nozzle heating, resulting in a beam with intermediate E_i, we have verified that heating the nozzle has no influence on the sticking probability. To determine the (spread in) kinetic energy of the O_2 in our beam, time-of-flight (TOF) experiments were performed with the movable mass spectrometer. To obtain a sufficiently low flux of oxygen (Air Products, 5.8 or Hoekloos 3.96 vol% O_2 in He, 4.6), we mixed gases feeding the expansion with an O_2 concentration less than 8%. In addition, the beam was chopped at high frequency ($\sim$ 250 Hz) by a chopper wheel with a 16% duty cycle. The (initial) sticking probabilities were determined with the fixed mass spectrometer using the King and Wells technique (KW)[8]. Our UHV system has a vacuum time constant for O_2 on the order of 0.05 s which causes a nearly stepwise initial increase of the partial O_2 pressure within the first second in all sticking probability measurements. It is followed by various typical coverage dependencies that last for 10^1 to 10^2 of seconds. A linear fit through the first few seconds of the data was used to accurately determine the sticking probability at $t = 0$ (as in chapter 3). No significant variations in S_0 were found in a period of two years and after several modifications to the setup had been made.

5.3 Results

5.3.1 Initial sticking probability

Figure 5.2 shows the initial sticking probability of O_2 on the Pt(553) surface (circles) for T_s = 200 K as a function of the incident kinetic energy. Maxwell distributions

for O_2 are added as lines for room temperature and temperatures common in car exhausts[1] to indicate the most relevant energy range. For comparison, the data for Pt(533) (squares[84]), Pt{110}(1x2) (diamonds[69]), and Pt(111) (triangles[20]) are also shown in this figure. For $E_i < 0.2$ eV, S_0 decreases with increasing incident energy. Although this trend is seen for all surfaces, the absolute values of S_0 for the Pt(553), Pt(533), and Pt{110}(1x2) surfaces are significantly higher as compared to the Pt(111) surface. Noticeably, the absolute values for these stepped surfaces coincide up to ~0.15 eV. Here we note that in previous experiments for H_2 dissociation on Pt(533) researchers in our group also have shown quantitative agreement between our group and the Hayden group[50,52]. Hence, the overlap is not accidental. For $E_i > 0.2$ eV, S_0 slowly increases, until a plateau is reached. The sticking probability for Pt(553) levels off to approximately 0.33, i.e. slightly higher than the value which was found for Pt(111)[19,20], whereas for Pt(533) S_0 converges to a significantly higher value of 0.425[84].

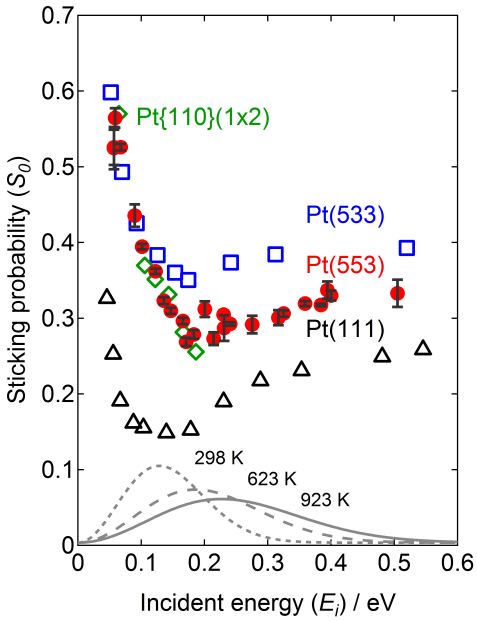

Figure 5.2: S_0 of O_2 on Pt(553) (circles, with error bars in y-direction), Pt(533) (squares[84]), Pt{110}(1x2) (diamonds[69]) and Pt(111) (triangles[20]) as function of incident kinetic energy. In all experiments the incident angle is normal to the surface and T_s = 200 K. Maxwell distributions for 298 (dotted), 623 (dashed), and 923 K (solid) are shown with arbitrary intensity.

Figure 5.3 shows the initial sticking probability as a function of surface temperature for the Pt(553) (circles), Pt(533) (squares[84]), Pt{110}(1x2) (diamonds[69]), and Pt(111) (triangles[20]) surfaces. For low incident kinetic energy (open symbols), S_0 generally decreases with increasing surface temperature. The values for $S_0(T_s)$ are again the same for Pt(553), Pt(533), and Pt{110}(1x2). They are significantly higher than for Pt(111), although the slopes ($^{dS_0}/_{dT_s}$) are rather similar. We note here that scrutinizing our data for Pt(553) shows that S_0 is actually temperature independent between 150 and 250 K within experimental uncertainty (0.56 $\pm$ 0.01). A drop with increasing temperature is only observed for $T_s > 250$ K.

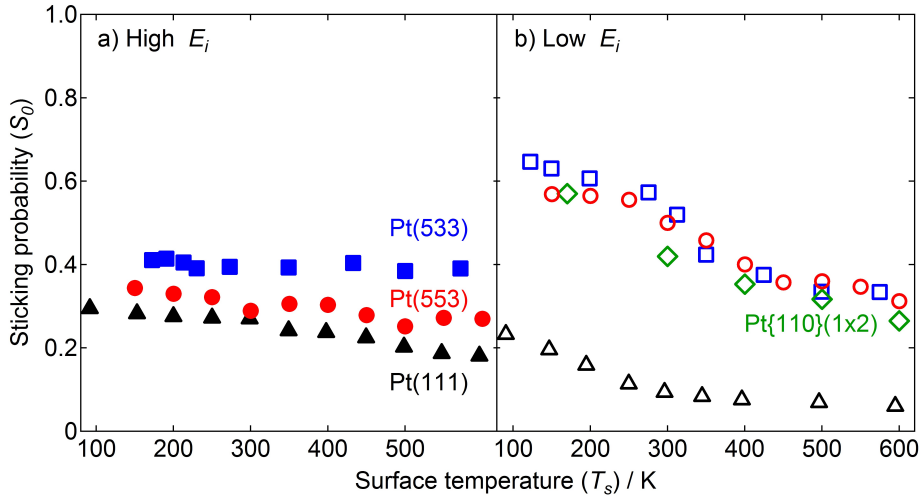

Figure 5.3: S_0 of O_2 on Pt(553) (E_i = 0.059 eV and 0.40 eV, circles), Pt(533) (E_i = 0.052 eV and 1.15 eV, squares[84]), Pt{110}(1x2) (E_i = 0.064 eV, diamonds[69]), and Pt(111) (E_i = 0.085 eV and 0.9 eV, triangles[20]) as a function of T_s.

At higher incident energy (filled symbols) S_0 is less dependent on the surface temperature. It still varies clearly for Pt(553) and Pt(111) and shows nearly the same values for $^{dS_0}/_{dT_s}$. However, S_0 for Pt(533) is significantly higher and seems nearly independent of T_s in comparison to the other surfaces. We note that the E_i at which this data was collected varies significantly for the individual surfaces. However, the near energy independence for $E_i > 0.40$ eV justifies the comparison.

Figure 5.4 shows S_0 as a function of the incident angle for the Pt(553) (circles) and Pt(533) (squares[84]) surfaces. The incident angle (Φ) is defined as the an-

gle between the supersonic molecular beam and the surface normal, where O_2 molecules impinge on the open side of the step for positive angles. As expected from the anisotropy of the Pt(553) and Pt(533) surface structures, S_0 shows an asymmetric behavior with a higher sticking probability for positive angles at all incident energies. For low E_i (open symbols), the Pt(553) surface shows a stronger angular dependence for S_0 than the Pt(533) surface. This effect is not due to the lower surface temperature used in our experiments as the same trend was observed for T_s = 225 K (not shown here). For higher values of E_i (filled) there are more striking differences between the Pt(553) and Pt(533) surfaces. Gee and Hayden deconvoluted the total signal for Pt(533) to separate the contributions from the terraces ($\Phi_\perp \approx -14°$) and steps ($\Phi_\perp \approx 40°$)[84]. For positives angles, the data for Pt(553) yield no suggestion how to separate contributions from the step edges and terraces. It shows a smooth, nearly angle independent trend, with a dip at Φ = 40°. This dip is a real feature of the data set and was observed consistently for multiple values of E_i.

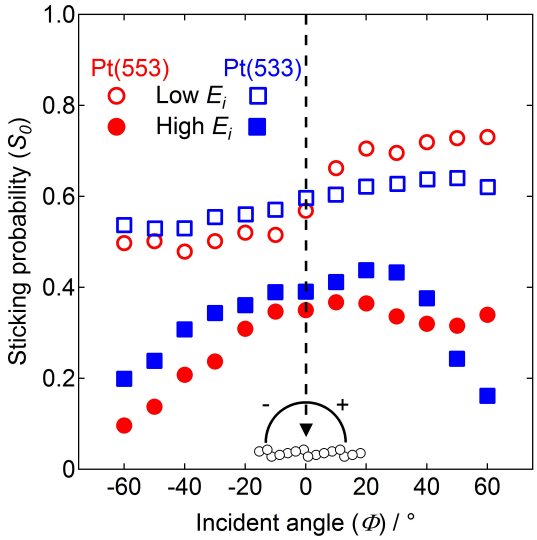

Figure 5.4: S_0 of O_2 on Pt(553) (E_i = 0.059 eV, open and 0.40 eV, closed circles at T_s = 150 K) and Pt(533) (E_i = 0.052 eV, open at T_s = 225 K and E_i = 1.15 eV, closed squares at T_s = 350 K[84]) as a function of the incident angle Φ.

5.3.2 Coverage dependent sticking probability

The data in figure 5.5 show the change of the sticking probability during the experiment for E_i = 0.059, 0.23, 0.32, and 0.40 eV (5.5a-d respectively) and for T_s = 150, 200, and 250 K. As the absolute maximum oxygen coverage for Pt(553) is not known and may depend on the incident kinetic energy and surface temperature, we have not converted the horizontal axis to a coverage in monolayers here. However, the data still reveal crucial information on the dynamics of oxygen sticking on Pt(553).

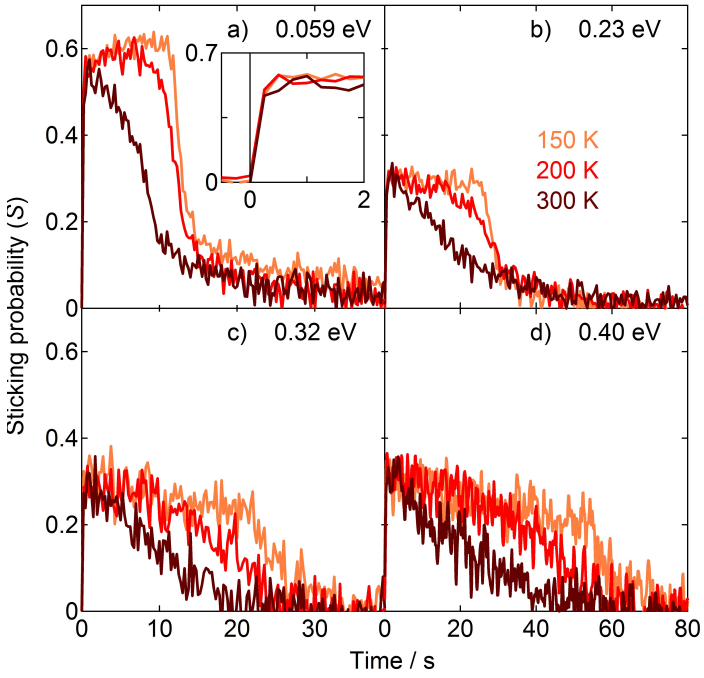

Figure 5.5: Change of the sticking probability of oxygen on Pt(553) during the experiment for T_s = 150 K (light), T_s = 200 K (red), and T_s = 250 K (dark) at Φ = 0 and a) E_i = 0.059 eV; b)E_i = 0.23 eV; c)E_i = 0.32 eV; d)E_i = 0.40 eV. The O_2 flux was not the same for the different beams. For a-c) the time axis is 0-40 seconds, for d) it is 0-80 seconds.

First we observe that at t = 0 the sticking probability steps up within a fraction of a second. This is a consequence of the convolution of the measurement with the vacuum time constant for O_2. Second, we note that S_0 (the intercept with the y-axis)

is quantitatively the same for T_s = 150, 200, and 250 K for all incident energies. Only beyond 250 K, S_0 drops with increasing T_s (see figure 5.3). Third, as plotted in the four panels, $^{dS}/_{d\theta}$ in the limit of θ = 0 seems the same for T_s = 150 and 200 K for all incident energies. It varies from being clearly positive to slightly negative. For T_s = 250 K, $^{dS}/_{d\theta}$ seems lower than the values at lower surface temperature and always negative. However, the inset shows that this difference between T_s = 250 K and the other traces is not present in the first two seconds of the experiment. We only show one inset, but the same overlapping traces occur in the first seconds of all panels, and the slope $^{dS}/_{d\theta}$ in the zero-coverage limit is exactly the same within each panel. The differences in coverage dependence only develop after the coverage has increased well beyond 0. Furthermore, we note that for the lowest surface temperatures, the sticking probability shows an abrupt change in slope after a certain number of O_2 molecules has impinged onto the surface. The abruptness decreases with increasing surface temperature. Finally, after the abrupt decrease, at low E_i it takes significantly longer to reach S = 0. This is most clearly seen in the slow decrease of the traces in figure 5.5a for longer times.

Figure 5.6 shows as a 3-D plot of $S(\theta,\Phi)$ for E_i = 0.059 eV and T_s = 150 K. This sticking surface was constructed from 13 individual coverage-dependent sticking measurements. We slightly smoothed the surface to reduce noise. The coverage is an arbitrary value calculated by integrating the multiplication of time and flux (as determined in a relative sense by the QMS current for $^{m}/_{e}$ = 32 while the molecular beam enters the chamber and impinges onto an inert flag) with the sticking probability. It is also corrected by a factor $cos(\Phi)$ for the larger surface area onto which the beam deposits oxygen for increasing angles. This yields a total obtained (maximum) coverage in these experiments that is independent of incident angle. The initial step-like increase in sticking at all angles is again a result of the convolution of our measurement with the vacuum time constant of O_2. This step-like increase is immediately followed by two different behaviors. For positive incident angles, where O_2 impinges into the step, the sticking probability is independent of coverage until some saturation level is reached and sticking plummets. For negative angles, where the downward step becomes increasingly invisible to the impinging molecule, the initial sticking probability is lower. However, sticking clearly increases with coverage. This behavior is maintained for a while after which the sticking probability also drops similar to the behavior at positive incident angles.

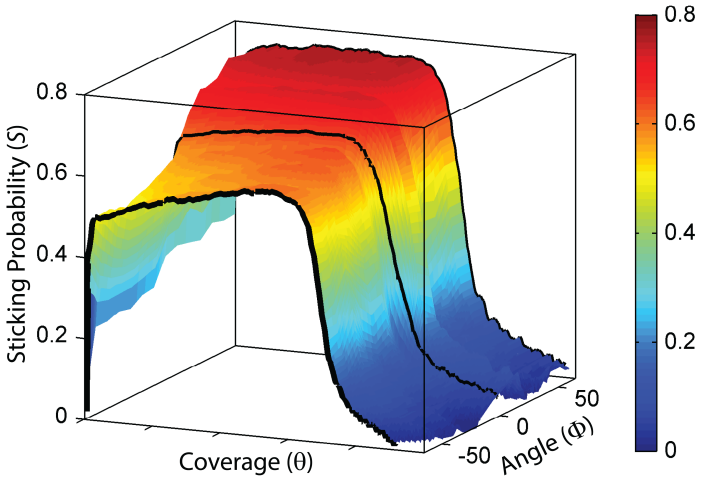

Figure 5.6: Sticking probability of O_2 on Pt(553) as function of θ and Φ for E_i = 0.059 eV and T_s = 150 K.

5.3.3 Thermal desorption

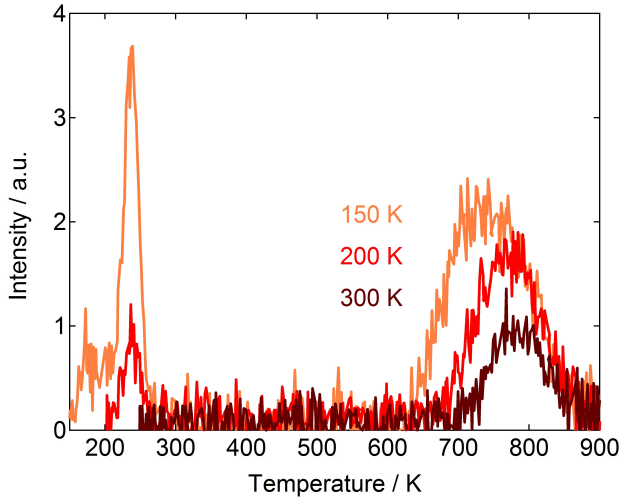

Figure 5.7: TPD spectra of O_2 desorption from Pt(553) recorded after KW experiments for T_s = 150 K (light), T_s = 200 K (red), and T_s = 250 K (dark) with a heating rate of 4.0 K/s.

Figure 5.7 shows temperature programmed desorption spectra obtained after a molecular beam impinged onto the Pt(553) surface until we observed no more sticking. The three traces were obtained for E_i = 0.059 eV at normal incidence and for T_s = 150, 200, and 250 K. The spectra show two desorption peaks between T_s = 150 K and T_s = 250 K as well as the previously studied associative desorption features for this surface at much higher temperatures[95]. Previous studies for O_2 desorption from Pt(111) that used an effusive source only show a single desorption feature near 150 K from a molecular state[97]. On that surface desorption occurs in parallel with dissociation. For Pt(111), vacuum oxidation by O_2 leads to a maximum coverage of 0.25 ML O/Pt, unless it is performed at considerably higher temperatures[98]. Stepped Pt surfaces yield additional desorption peaks ascribed to molecular adsorption at or near steps[85,86,90,91]. The peak between 220 and 250 K is therefore likely due to step-bound O_2. In our experiments, the peaks from molecular states disappear with increasing surface temperature. Wang *et al.*[85] and Rar and Matsushima[86] found similar large molecular desorption peaks for Pt(533), while Gee and Hayden only reported a considerably smaller peak[84].

TPD studies following upon adsorption from a supersonic molecular beam may not relate quantitatively to the adsorption from the beam. The total adsorption as calculated by integrating the multiplication of time and flux with the sticking probability may contain a contribution of adsorption into meta-stable sites that desorb in between stopping the beam and starting the temperature ramp. The isothermal desorption from weakly-bound states 'while not measuring' causes a quantitative discrepancy that renders us unable to relate our KW and TPD data quantitatively. On the other hand, part of molecularly-bound O_2 created at low T_s, may also dissociate during the consecutive temperature ramp. It reappears in the associative desorption regime of the TPD spectrum. The increase in the O_2 associative desorption between 600 and 900 K for experiments performed at 200 and 150 K relative to 250 K is most likely a result from this process.

5.4 Discussion

5.4.1 Initial sticking probability

Based on the previous studies using Pt(111), O_2 adsorption is generally described by:

$$2\mathrm{O}_{\mathrm{chem}} \overset{3}{\rightleftharpoons} \mathrm{O}^{\mathrm{n-}}_{2,\mathrm{chem}} \overset{2}{\rightleftharpoons} \mathrm{O}_{2,\mathrm{phys}} \overset{1}{\rightleftharpoons} \mathrm{O}_2(\mathrm{g}) \qquad (5.1)$$

where $\mathrm{O}^{\mathrm{n-}}_{2,\mathrm{chem}}$ describes molecular states, such as the peroxo- and superoxo-like states[19]. These may act as precursors to dissociation while desorption from these states is also possible. The maximum coverage of molecular O_2 exceeds the atomic coverage of O on Pt(111)[97,99]. Part of the $\mathrm{O}^{\mathrm{n-}}_{2,\mathrm{chem}}$ adsorbed at low temperatures desorbs around 150 K while another part dissociates creating a (2x2) $\mathrm{O}_{\mathrm{chem}}$ overlayer. The additional low temperature desorption feature between 220-250 K observed in our TPD spectra for Pt(553) (figure 5.7) and Pt(533)[84–86] suggests that additional molecular states exist at step edges, likely of similar nature but more strongly bound than to (111) terraces. These molecular states may be similar but are not likely identical to molecular states appearing in potential energy surfaces (PES) for O_2/Pt or in sticking probability measurements in the zero-coverage limit. They are likely affected by interaction with co-adsorbed $\mathrm{O}^{\mathrm{n-}}_{2,\mathrm{chem}}$ or $\mathrm{O}_{\mathrm{chem}}$.

Sticking probability measurements, as performed in this study, do not distinguish between final states. The initial sticking probability is simply a summation of all possible parallel and consecutive adsorption pathways occurring on a time scale faster than the measurement:

$$\begin{aligned} S_0 = {} & S_0^{direct}(\mathrm{O}_{2,\mathrm{phys}}) + S_0^{indirect}(\mathrm{O}^{\mathrm{n-}}_{2,\mathrm{chem}}) \\ & + S_0^{indirect}(\mathrm{O}_{\mathrm{chem}}) + S_0^{direct}(\mathrm{O}^{\mathrm{n-}}_{2,\mathrm{chem}}) + S_0^{direct}(\mathrm{O}_{\mathrm{chem}}) \end{aligned} \qquad (5.2)$$

Here, individual contributions are ordered as numbered in reaction 5.1. Equation 5.2 also holds for non-initial conditions, although adsorption energies of atomic and molecular states may alter with coverage.

The physisorbed state is not stable at any experimental surface temperature in this study and its sole contribution to S_0 from reversible reaction 1.1 is zero[94]. However, the physisorbed state may be passed through for indirect molecular chemisorption, i.e. reaction 1.2. As adsorption on Pt(111) at low energies shows a negative dependence on incident energy, an indirect sticking mechanism into a chemisorbed state occuring via the physisorbed state is generally invoked[19,20,24]. The subsequent increase of S_0 with E_i is often argued to represent an additional activated

pathway to adsorption. For Pt(111), this is reaction 1.4, i.e. direct sticking into a molecular state. For surface temperatures exceeding ∼200 K, this chemisorbed and equilibrated O_2 either dissociates along an activated path, i.e. reaction 1.3, or desorbs back into the gas phase. This competition explains the T_s dependence at high E_i for Pt(111).

While this picture of O_2 adsorption was constructed in the previous century and mostly based on experimental studies, theoretical studies are still debating whether the physisorbed state on Pt(111) is a crucial ingredient to explain the kinetic energy dependencies. A recent molecular dynamics simulation, based on a classical reactive force field approach, includes a physisorption well of ∼0.04 eV, a molecular chemisorption well of 0.35 eV and a very high barrier to dissociation from the latter well in a top-bridge-top geometry[81]. The study finds that sticking in the low energy regime proceeds via steering and trapping in the physisorption well. It reproduces the energy-dependence on sticking, including the dip in reactivity near 0.2 eV, and results from an older O_2 scattering study[100] reasonably accurately. On the other hand, a previous tight-binding molecular dynamics study reproduced kinetic energy and surface temperature trends without such a physisorption well[23]. E_i-dependent steering and energy transfer from the surface to the molecule at finite surface temperatures were indicated as the origins for the experimentally observed trends.

The similar energy and surface temperature dependencies for sticking on Pt(533) were, by comparison to the previous experimental studies for Pt(111), interpreted to suggest, at least in part, the same two sticking mechanisms; indirect adsorption via the physisorbed state and activated direct adsorption into molecular states. The significantly higher values for S_0 at low incident energy for Pt(533) were ascribed to additional direct chemisorption at the step and increased conversion of a physisorbed state to the chemisorbed state by the step. An increased reactivity at high incident energy was ascribed to an additional channel, i.e. direct, activated dissociative adsorption at the (100) step (reaction 1.5). The clear peak at the [100] normal in the angular dependence for high incident energy (see figure 5.4), was considered a fingerprint of this channel.

With this in mind, we turn to our results for O_2 sticking on Pt(553) and the comparison of data to those obtained for other Pt surfaces. We focus on the low E_i regime first.

5.4.2 Sticking at low E_i

From figure 5.2, we note that the same characteristic features appear in the initial adsorption of O_2 on Pt(553), Pt(533), Pt{110}(1x2), and Pt(111). For $E_i < 0.2$ eV the initial sticking probability strongly decreases with increasing incident energy. Also, a general decreasing trend with surface temperature is observed in this energy range (figure 5.3), although S_0 for Pt(553) is actually independent of surface temperature between 150 and 250 K. Thereafter it drops steadily as it does for all other Pt surfaces. Furthermore, the absolute values of $S_0(E_i < 0.15$ eV, $T_s)$ are equal for Pt(553), Pt(533), and Pt{110}(1x2), and significantly higher than for Pt(111). For the stepped surfaces, $S_0(\Phi)$ shows a smooth dependence, favoring an approach into the step (figure 5.4).

The similarities, especially for Pt(553) and Pt(533), may easily persuade us to adopt an explanation based on previously suggested direct and indirect mechanisms for sticking. Gee and Hayden introduced the idea of parallel sticking mechanisms to explain high sticking at low incident energy data for Pt(533) as compared to Pt(111)[84]. They reasoned that a physisorbed precursor state would be more efficiently turned into a chemisorbed state on Pt(533) because of the high step density. Using a hard cube model for data at $E_i \simeq 0.05$ eV, they found this mechanism to be responsible for 0.3 of the total initial sticking of $\sim$0.6. Direct adsorption into a molecular chemisorbed state at the (100) step edge of Pt(533) was considered to contribute the other half. This direct molecular adsorption was indicated to be the same mechanism as one of the two parallel mechanisms accounting for sticking at high incident energy, i.e. direct molecular sticking (reaction 1.4). Oddly, this mechanism was considered to be activated in order to account for the increase in reactivity with increasing energy. This seems in contradiction to a mechanism contributing half of $S_0 \simeq 0.6$ at an incident energy of only 0.05 eV.

We believe that the behavior of the stepped surfaces at low energy is indeed a result of parallel sticking mechanisms. However, we expect that direct molecular sticking at the step edge in a non-activated process. At the upper edge of the step, the molecular chemisorbed state is calculated to be bound on the order of 0.5-1.0 eV more strongly than at terrace sites[87]. By the principle from Bell[101], Brønsted[102], Evans, and Polanyi[103] (BEP principle), this doubling of the well depth should drag any barrier to molecular chemisorption down. We expect this to be at least several tenths of an eV. As the impinging molecule at low kinetic energies will mostly follow

the minimum energy path and steering seems efficient[23,81], we see no reason why direct molecular adsorption should be activated at the step. In parallel, sticking will also occur on (111) terrace sites, very similar to sticking on the 'infinite' (111) plane, irrespective whether it proceeds via a physisorbed state or via direct steering into a chemisorbed molecular state. Finally, the cusp of the step may very well be some intermediate zone where adsorption is not non-activated, but still different from adsorption on terrace sites.

For H_2, experiment and theory suggest that the unit cell of a stepped surface may simply be divided into various regions, where the local potential dictates which adsorption mechanism is dominant[50,52,72,73]. This leads to a weighted average sticking probability that quantitatively represents the various ways available for an impinging molecule to stick to a non-uniform surface. Using a series of (100) stepped Pt surfaces, researchers in our group have shown that a simple model based on the results from a three-atom wide terrace, quantitatively predicted the measured sticking probability for all other stepped surfaces and Pt(111)[52]. The model was not very sensitive to the exact assumed partitioning between step and terrace areas. Based on that approach, we may expect that the Pt(553) surface is reasonably well described as consisting for $\sim$50% of an area dominated by the step (upper area and lower area) and for $\sim$50% as acting like the Pt(111) surface for O_2 sticking. Hence, the total S_0 can be rewritten as

$$S_0^{553} \simeq 0.5 \cdot S_0^{step} + 0.5 \cdot S_0^{terrace} \tag{5.3}$$

The step and terrace contributions may result from various mechanisms that (for reasons of simplicity) we here refer to as direct and 'indirect'.

$$S_0^{step} = S_{0,direct}^{step} + S_{0,indirect}^{step} \tag{5.4a}$$

$$S_0^{terrace} = S_{0,direct}^{terrace} + S_{0,indirect}^{terrace} \tag{5.4b}$$

Figure 5.8 shows the results of our model that ascribes the measured sticking probability for Pt(553) to represent a weighted average of two contributing areas of roughly equal size as schematically indicated in the inset. We have applied a polynomial fit to published Pt(111) data (solid black line). From this fit and a

polynomial fit through our measured data for Pt(553) (red data with a solid red line), we calculate the local energy-dependent sticking at the (110) step (solid blue line). We then take these two local energy-dependent sticking probabilities for step and terrace, multiply them by 0.5, and separate their contributions to the measured data further into different sticking mechanisms.

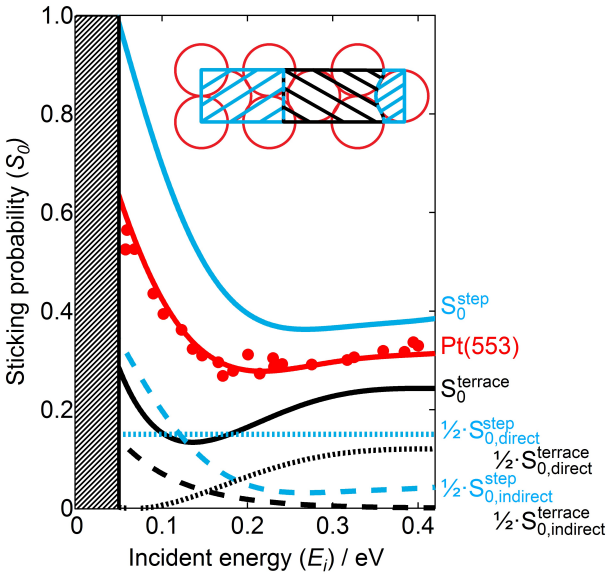

Figure 5.8: Deconvolution of the initial sticking probability into contributions from the (110) step edges and the (111) terraces.

For the contribution of the step, we argued that non-activated direct adsorption takes place. We estimate this partition directly from the difference between the reactivity observed for Pt(111) and Pt(553) (see discussion below) and expect it to be roughly energy-independent. This contribution (dotted blue line) leaves an energy-dependent remainder (dashed blue line) that must be ascribed to another sticking mechanism for O_2 molecules impinging at the bottom of the step edge. In equation 5.4 and in figure 5.8 we refer to this contribution as 'indirect'. The contribution from the (111) terrace is also separated into two components as suggested previously [19,21,24]. We have used an exponential decay to fit the low E_i data. It represents the indirect component that others quantify using a hard cube model [24,84].

In comparing the individual contributions, we find that direct processes have

roughly the same maximum value for step and terrace. Whereas direct adsorption into a molecular state is non-activated at the step, it is activated for molecules impinging on the terrace. For molecules sticking with a negative energy dependence, the ones impinging at the bottom of the step have roughly twice the chance of sticking compared to those impinging onto the terrace. Overall, this rough model is not very different from those proposed previously [19,24,84]. However, we now consider three contributions to sticking at low incident energy on the stepped surface. The two 'indirect' mechanisms are replaced by a fourth mechanism with increasing energy.

We consider the qualitative consequences of this model for other observed dependencies at low incident energy. The negative surface temperature dependence beyond 250 K may be explained by the large contribution of two 'indirect' mechanisms. Whether these are truly indirect and proceed via a physisorbed state can not be concluded from our sticking probability measurements in the zero-coverage regime. The coverage dependencies at low incident energy and low surface temperatures show the expected features of a long-lived precursor state. Sticking even increases with coverage for the lowest surface temperatures. However, the difference in perception that is exemplified by the inset in figure 5.5, remind us that mechanisms contributing at larger coverages may not be the same as those operating on the clean surface. The inset shows that the mechanisms contribution to sticking at zero coverage are surface temperature independent up to 250 K. It is only at higher coverage that a surface temperature dependence appears. This may be interpreted to show that sticking occurs directly into chemisorbed states as S_0 only drops at surface temperatures when all these states have become unstable.

The angle dependence in figure 5.4 argues for the separation of sticking through 'indirect' mechanisms at terrace and step sites in our model. As the top of the step, where chemisorption may occur into a deep molecular well, protrudes from the (553) plane, one would not expect a significant or strongly asymmetric dependence on incident angle for this direct mechanism. Indirect sticking at the (111) terrace should show a symmetric dependence around the [111] normal at -12.3°. Hence, the asymmetry and increase at positive angles imply that molecules impinging into the lower part of the step have a different interaction with the surface than those impinging on (111) sites.

The combined angle and coverage-dependencies in figure 5.6 are in this regard also intriguing. We interpret the difference in behavior for negative and positive

incident angles as a signature that step-bound molecular O_2 provides additional corrugation with the ideal mass match for subsequently impacting O_2 molecules. In other words, step-bound O_2 molecules may aid indirect sticking by acting as efficient collision partners. This effect would increase with increasing negative impact angles. For positive impact angles, they will have less influence as the step itself already provides corrugation and efficient means for slow impacting molecules to loose their kinetic energy and momentum.

Finally, we consider whether our model explains both the similarities and minor differences between the stepped surfaces. We believe the origin for the overlap in S_0 for Pt(533), Pt(553), and Pt{110}(2x1) points to a dominant contribution of the step to the total sticking in the low energy regime. The length of the unit cell, hence the step density, is the same to within 10% for these surfaces. This implies that the number of impact sites leading to enhanced 'indirect' sticking through impact at the bottom of the step edges, e.g. by enhanced kinetic-to-rotational energy transfer[72,104], is approximately the same for all stepped surfaces considered here. Also the number of top edge sites where O_2 molecules experience a higher binding energy and where direct non-activated adsorption may occur, is nearly the same for these surfaces. Here, it is noteworthy that not only the step density but also the macroscopic work function is (nearly) the same for these three stepped surfaces[105,106]. The only difference in dependencies that we find at lower energy is the slightly higher sticking for Pt(553) for positive impact angles. We expect that details of the PES, governing the extent of momentum and energy transfer, manifest themselves here.

5.4.3 Sticking at high E_i

Our proposed model for the observed kinetic energy dependence suggests that with increasing incident energy the 'indirect' mechanisms are replaced by activated, direct sticking at the (111) terrace. At the highest incident energies, roughly half of the molecules stick if their trajectory directs them into a chemisorbed state at the top edge of the step. The other half sticks as a consequence of having enough kinetic energy to overcome an (apparent) activation barrier when impinging onto a (111) terrace site. The contribution of the direct, non-activated mechanism was estimated from the maximum difference occurring between Pt(111) and Pt(553) in the regime where the 'indirect' mechanisms start to fail. This is $\sim$0.15 at 0.2 eV.

Considering the physical size of the top of the edge in proportion to the unit cell of Pt(553), this value also represents a reasonable fraction of trajectories impinging onto this site. Furthermore, the estimate does not lead to an unphysical value, i.e. $S_0^{step} > 1$. Here, we note that the behavior below $\sim$0.05 eV is simply unknown and, with standard supersonic molecular beam methods, impossible to determine. Finally, we do not consider the estimate of 0.15 very accurate, although it can also not be very different within our model. A very similar value was found for direct non-activated H_2 dissociation onto the top of Pt step edges[52,73].

In comparison to Pt(111) and Pt(533), sticking on Pt(553) is intermediate at the highest kinetic energies. Also, in contradiction to the behavior at low kinetic energy, the angle dependence for the two stepped surfaces is not very similar. For Pt(533), a clear 'bump' is observed near the [100] normal on top of a smooth trend. The angle dependence and weak T_s dependence were interpreted to indicate that the (100) steps on Pt(533) facilitate direct activated dissociation at high E_i[84]. The data for Pt(553) seems rather insensitive to the impinging angle for positive angles. We only observe a small but reproducible dip appearing at $\sim$40°. Also the temperature dependence in figure 5.3 at high incident energies varies between the stepped surfaces. Pt(533) is significantly less dependent than Pt(553). The latter actually resembles the behavior of Pt(111) more closely. Both observations justify that our model does not include direct dissociative adsorption at high kinetic energies.

The difference between the two step types is also echoed by our previously published TPD data for these surfaces. Associative desorption from Pt(533) occurs at higher temperatures than for Pt(553). This indicates a more strongly bound atomic state on the (100) step[95]. This represents itself also in a weaker tendency for atomic oxygen bound at the (100) step edge to become hydrogenated to hydroxyl as compared to O_{chem} bound to (110) steps and the (111) terrace[95,107,108]. A more strongly bound atomic state would, by the BEP principle, reduce the barrier between molecularly chemisorbed O_2 and O_{chem}. Apparently, the barrier reduction for the (100) step is large enough to allow for direct dissociation. The only minor indication that it may also occur on Pt(553) at higher E_i is the slight upturn in $S_{0,indirect}^{step}$. This may be wrongly ascribed and actually reflect a very small contribution of direct dissociation at high E_i. Obviously, spectroscopic identification of the products would be conclusive. Unfortunately, we are not currently capable of producing such data.

Previous groups have used a simple kinetic model to extract the trapping probability (α_{mc}), relative reaction barriers ($E_d - E_a$, with subscripts d and a indicating

desorption and dissociation respectively) and frequency factors ($^{\nu_a}/_{\nu_d}$) from the experimental data at high incident energies, by assuming three different adsorption states (O_{chem}, $O^{n-}_{2,chem}$, and $O_{2,phys}$) and two distinct reaction pathways (reaction 5.1.2 and 5.1.4). This has been done for Pt(111), Pt(533), and Pt{110}(1x2)[19,20,24,69,84]. For reason of completeness, we have applied this model to our data. Assuming a trapping probability of 0.32, we find similar values ($E_d - E_a$ = 0.054 eV, and $^{\nu_a}/_{\nu_d}$ = 1.18) as for the other surfaces. However, we question how reliable this model is. Increased well depths of atomic and molecular states at the stepped surfaces combined with lower barriers to dissociation reduce the lifetime of precursor states. This competes with equilibration, which is at the heart of the kinetic model. Recent high dimensionality dynamical calculations for Pd(100) that explicitly include phonon excitation[42], and where the molecular chemisorption energy is very similar to the value calculated for Pt steps[87], show no signs of equilibration. Furthermore, as input for this model α_{mc} is assumed from high E_i and low T_s data. Keeping this in mind, we believe that the numbers resulting from this model should not be used as anything more than rough estimates if appropriate at all.

5.5 Conclusions

Combining the observations from the experiments for Pt(553), Pt(111), and Pt(533), we suggest the three qualitative 1-D PESs shown in figure 5.9a. For clarity, we do not extend atomic and molecular chemisorption potential curves along the x-axis to high values. The inset shows the expected relative dissociation barriers. Figure 5.9b shows the locations and orientations of $O^{n-}_{2,chem}$ and O_{chem}. For molecular O_2, both TPD experiments (for Pt(331)[90] and Pt(311)[91]) and DFT calculations[87] (Pt(221) and Pt(211)) find that $O^{n-}_{2,chem}$ is orientated parallel to the step edge.

We highlight the crucial similarities and differences between the three potentials. First, the weakly bound physisorption state (0.08 eV per O_2[81]) is probably not notably different for the three surfaces. However, the two different step types bind $O^{n-}_{2,chem}$ significantly stronger than the (111) terrace (top-fcc-bridge, 0.6 eV). The binding energy for the two step edges is similar ($\sim$1.5 eV). The atomic states differ between all surfaces. Both step types bind O_{chem} more strongly than Pt(111). The associative desorption temperature of $O_{chem,step}$ for Pt(533) is 36 K higher than for Pt(553)[95]. This suggests that the $O_{chem,step}$ potential well is deepest for the (100)

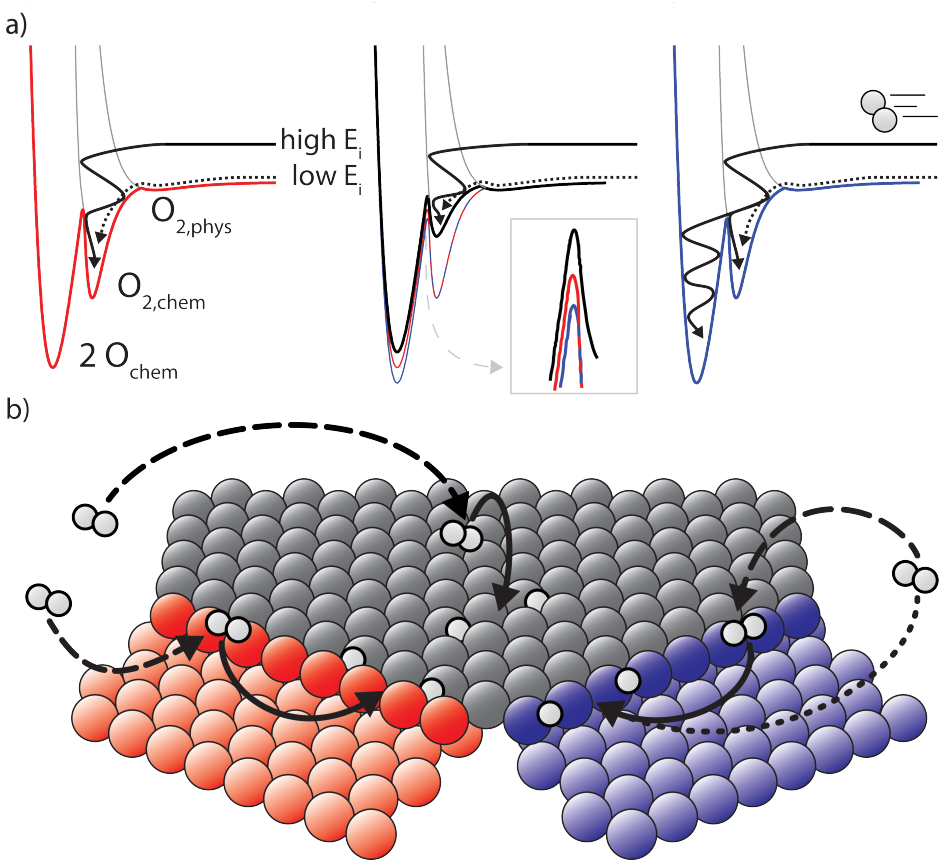

Figure 5.9: a) Qualitative 1-D PES for O_2 adsorption on the Pt(553) (red), Pt(111) (black), and Pt(533) (blue) surfaces; b) Model surface indicating the experimentally observed adsorption pathways and geometries for the different surface structures.

step. These observations are supported by DFT calculations which report binding energies of 2.2, 2.4, and 2.6 eV for 2 O_{chem} on Pt(111) (fcc hollow), Pt(221) (step fcc hollow), and Pt(211) (step bridge) respectively[87]. The BEP principle requires that the barrier for dissociation from the molecular state is reduced more on the (100) step type than on the (110) step type. This qualitatively explains why direct dissociative adsorption (reaction 5.1.5) is only observed for Pt(533). The reaction paths drawn in figure 5.9a visualize that for the Pt(111) and Pt(553) surfaces at low and high E_i O_2 dissociates only via $O^{n-}_{2,chem}$, whereas on Pt(533) a channel to direct dissociative adsorption has opened.

Summarizing, we have shown that using a simple model it is possible to qualitatively explain the features of our data for adsorption of O_2 on Pt(553). The total sticking probability has been described in terms of contributions from four different reaction pathways. Two of these pathways are decreasing with increasing E_i, the third is activated, and the fourth is independent of E_i. This description is consistent with adsorption and desorption data from experiments and theory and may likely be applicable to similar systems.